

Article

Coupling between Benthic Nutrient Cycling and Pelagic Phytoplankton Community in Taiwan Strait in Spring 2018

Xiaowen Li ^{1,2}, Xiaojie Chai ^{1,2} , Lingling Zheng ¹, Qinghui Deng ^{1,2}, Xiaoyan Chen ¹, Qi Zhang ¹, Lingling Wan ¹, Chunlei Song ¹, Lirong Song ¹, Yiyong Zhou ¹ and Xiuyun Cao ^{1,*}

¹ State Key Laboratory of Freshwater Ecology and Biotechnology, Key Laboratory of Algal Biology, Institute of Hydrobiology, Chinese Academy of Sciences, Wuhan 430072, China; lixw@ihb.ac.cn (X.L.); chaixj@ihb.ac.cn (X.C.); zhengll@ihb.ac.cn (L.Z.); dengqinghui@ihb.ac.cn (Q.D.); chenxiaoyan839@163.com (X.C.); zhangq@ihb.ac.cn (Q.Z.); wanlingling@ihb.ac.cn (L.W.); clsong@ihb.ac.cn (C.S.); lrsong@ihb.ac.cn (L.S.); zhouyy@ihb.ac.cn (Y.Z.)

² University of Chinese Academy of Sciences, Beijing 100039, China

* Correspondence: caoxy@ihb.ac.cn; Tel.: +86-027-6878-0221/0123

Received: 13 September 2020; Accepted: 15 October 2020; Published: 18 October 2020



Abstract: Although the nutrient as a driving force for the red tide was intensively studied, the spatial patterns of the phytoplankton community and its response to benthic nutrient cycling remain unclear. We determined the pelagic phytoplankton community and its extracellular alkaline phosphatase qualitatively using enzyme-labeled fluorescence (ELF) technique, concomitantly with the concentrations of phosphorus (P) and nitrogen (N) in the water and sediments in the Taiwan Strait in spring 2018. A total of 30 phytoplankton genera were identified with a higher abundance of the abundance of *Prorocentrum* and *Trichodesmium* being observed at the north coast and the center of the southern strait, respectively. Both phytoplankton abundances and *Trichodesmium* were negatively correlated with the ratios of dissolved inorganic N and ammonium to soluble reactive P (DIN/SRP, NH_4^+ /SRP) in the bottom. Furthermore, the ELF-labeling percentage in *Trichodesmium* was negatively correlated with total P and SRP but positively correlated with TN/TP, DIN/SRP, and NH_4^+ /SRP in the bottom. In contrast to high DIN/SRP of the surface, lower DIN/SRP in the bottom was owing to a high P release potential and weak sequestration of P as evidenced by the distribution of P solubilizing bacteria and P content. Our findings indicated that the benthic nutrient regime might shape the structure of the pelagic phytoplankton community.

Keywords: Taiwan Strait; *Trichodesmium*; alkaline phosphatase; imbalanced nutrient; pelagic-benthic coupling

1. Introduction

As primary producers, marine phytoplankton play important role in photosynthetic carbon fixation and supporting the structure and function of the ecosystem. On the other hand, marine ecosystems have suffered from significant increases in the incident of algal bloom, which is usually called red tide [1]. Marine phytoplankton in terms of composition and abundance were directly related to global climate change, nutrient loading, and hydrological processes, such as coastal current, upwelling current, warm current, and the intruding water [2]. Concentration and ratio of primary production limiting nutrients, e.g., phosphorus (P) and nitrogen (N), play important role in regulating phytoplankton composition [3]. Benthic upwelling, diffusion, and stratification greatly affect the nutrient regime in the water column and therefore can modify also the phytoplankton composition. The pelagic and benthic region were closely related. For example, in the Swan River estuary, chlorophyll *a* (Chl *a*) concentration in the surface water

decreased with the elevating concentrations of nitrate (NO_3^-) and total phosphorus (TP) in bottom water [4]. The high primary productivity in the North Sea in summer was attributed to the diffusion of NO_3^- and ammonium (NH_4^+) from the bottom to the thermocline layer [5]. Dinoflagellate bloom in early summer in the East China Sea was triggered by the upwelling with abundant bioavailable P from the bottom [6]. Phosphate releasing bacteria played an important role in the P release process [7]. Close coupling between the benthic nutrient regime and pelagic phytoplankton composition is realized, while how benthic nutrients regulate pelagic nutrient regimes and phytoplankton remains to be fully characterized.

The phytoplankton community responds to nutrient supply by altering its composition. N_2 -fixing cyanobacteria are tended to dominate phytoplankton with excessive P relative to N inputs (or low N:P ratios) by fixing atmospheric N_2 to support the N requirements of bloom populations [8]. The biochemical adaptation by phytoplankton to low ambient nutrient supply could be a significant competitive advantage. For example, the success of picocyanobacteria in oligotrophic environments might owe to their biochemical composition adjusts by using sulfolipids instead of phospholipids [9]. Phytoplankton enriched in polyphosphate at low P could dominate the phytoplankton in the ultra-low-P Sea [10]. Phytoplankton such as some dinoflagellates evolved diverse dissolved organic P utilization strategy including endocytosis and producing alkaline phosphatase to hydrolyze extracellular dissolved organic P molecules might play critical roles in their bloom formation [11]. Concomitantly, the biochemical response of phytoplankton to ambient P was determined using the enzyme labeled fluorescence (ELF) technique, which is an accurate tool to indicate phytoplankton phosphate stress in natural phytoplankton [12]. However, the link between the biochemical responses of phytoplankton to benthic nutrient supply has been scarcely described.

Taiwan Strait (TWS) is located between the South and the East China Sea functioning as a shelf-channel, whose unique hydrology, climate, geological and geomorphologic features were created by the shape with wide terrain in the south and narrow in the north, as well as the inflow of rivers on both sides of the strait. Consequently, TWS is characterized by a marine sedimentary environment and high-quality fish resources [2]. In recent years, some worrying changes have taken place in the ecological environment of TWS, e.g., most of the traditional high-quality fish resources have been greatly reduced, the content of nutrients on the coast was intensified and the occurrence of red tide was frequent [13]. Previous researches on the phytoplankton of the TWS mainly concentrated on the effects of upwelling systems of the western region during the summer [14]. In TWS, the seasonal trend of phytoplankton is not well known although spring represents the period of greatest reproduction of microalgae. In situ field tests in the western TWS verified the limitation of nutrients to the growth of phytoplankton in the upwelling system and its regulation on the phytoplankton community structure [15]. However, which nutrient (N or P) limited the phytoplankton in the upwelling has not been fully analyzed. A systematic description of the response of phytoplankton communities in surface water to the concentration and composition of N and P in bottom water would be conducive to deeply understand the nutrition sources of primary producers, to explain their spatial and temporal patterns.

The aims of this study were (1) to supplement the records of phytoplankton communities in the TWS in spring and to improve knowledge of the spatial and temporal patterns; (2) to have an insight into the regulation of phytoplankton community by nutrient status; (3) to reveal the relationship between the benthic nutrient status and the pelagic characteristics of the phytoplankton community. We systematically described the abundance and composition of phytoplankton in different transects of the TWS in spring 2018. The relationship between the benthic and surface nutrient status and the response of pelagic phytoplankton was analyzed.

2. Materials and Methods

2.1. Study Area and Sampling Collection

Taiwan Strait (TWS) is located between Fujian Province and Taiwan Province in China. The length of the TWS is about 370 km, the north mouth is about 200 km wide and the south mouth is about

410 km wide, with a total area of about 80,000 km². 27 stations of 6 transects were investigated onboard the R/V Yanping 2 in the western TWS in spring from 24th to 28th March and 10th to 15th, April 2018 (Figure 1). Six transects were set vertically to the coastline and named as transects D, E, and F in the north, and transects A, B, and C in the south. The water depth of the northern region ranged from 15–64 m, while in the south is 9–2305 m (Supplementary Table S1). In addition, each transect was divided into the coast and center region. Surface and bottom water samples were collected in the southern TWS (transects A–C). Surface water samples and sediment samples were collected in the northern TWS (transects D–F). Sediment samples were collected using a box corer deployed from the R/V Yanping 2. Water samples were collected with a SeaBird Electronics (SBE917 Plus) CTD system. All samples were processed on board.

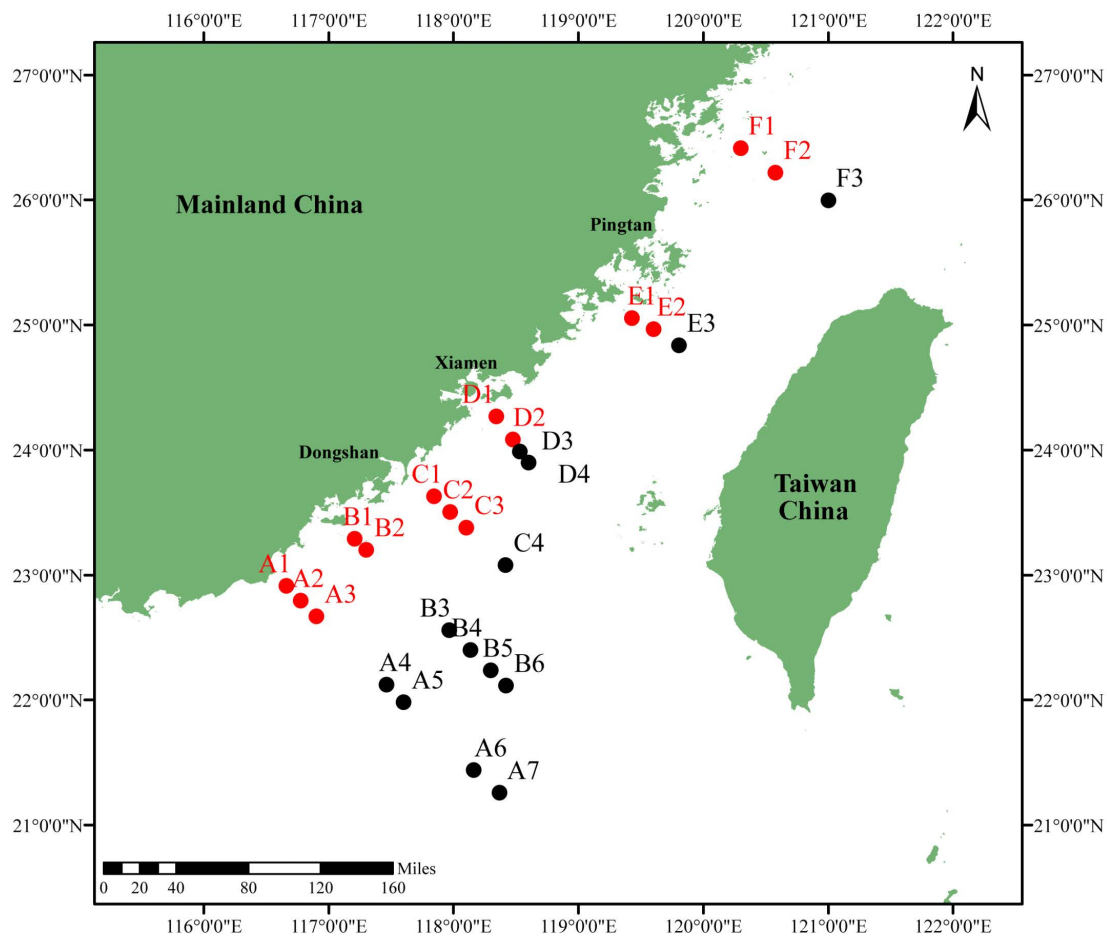


Figure 1. Map of the sampling stations in Taiwan Strait. The red dots indicate coastal stations while the black dots indicate the center in this study. Coastal and center regions were divided according to the distance of the transect from the beach, considering as a center region the one farther than 50 miles.

2.2. Phytoplankton Analysis

Phytoplankton samples were collected using a 20 μ m mesh plankton net and preserved in 3% neutralized formalin for further analysis. Only surface phytoplankton was classified to genus according to cell morphology. Numerical analysis was carried out using a microscope and phytoplankton was identified according to the illustrations by Guo [16].

2.3. Enzyme Labelled Fluorescence Measurements

Extracellular alkaline phosphatase (APase) was detected using ELF[®] 97 phosphate (ELFP, InvitrogenTM) in the phytoplankton according to the protocol [17,18]. 0.5 mL incubations were started

by adding the ELFP solution (final concentration 27 μM) and samples were incubated at 25 °C for 2.5 h. Each incubation was terminated by transferring the sample to a filter holder (diameter 7 mm) with a membrane filter (Millipore, 0.22 μm pore size). The filter with retained algae was placed on a microscope slide, embedded it with the anti-fading reagent Citifluor AF1 (Citifluor, London, UK), and covered with a cover slide for microscopic inspection (Olympus BX51FL).

2.4. Chemical Analysis

Total phosphorus (TP) was performed according to the digestion methods [19]. Analysis of total nitrogen (TN) followed the method reported by Standard Methods [20]. Soluble reactive phosphorus (SRP) measurement was determined following the molybdate blue method [21]. Analyses of different forms of N (NH_4^+ , NO_2^- and NO_3^-) followed the method reported by Standard Methods [20]. $\text{DIN} = \text{NH}_4^+ + \text{NO}_2^- + \text{NO}_3^-$.

Sediment P fractionation including iron-bound P ($\text{Fe}(\text{OOH})\sim\text{P}$), calcium-bound P ($\text{CaCO}_3\sim\text{P}$), acid-soluble organic P (ASOP), and hot NaOH-extractable organic P (Palk) were measured through Golterman [22]. P adsorption isotherm experiments were determined according to the method modified by Istvanovics [23]. The sediment samples were incubated with 0.01 mol/L KCl containing 0, 0.1, 0.5, 1, 5, 10, 20, 25, 30, 40 and 50 mg P/L KH_2PO_4 . The tubes were shaken for 24 h at 25 °C, centrifuged at 3000 rpm for 10 min, and filtered through 0.45 μm cellulose acetate membrane. Phosphate that disappeared from the solution was considered to have been adsorbed by sediments. Maximum adsorbed P concentration (Q_{max}) was obtained according to the Langmuir equation [24].

Inorganic P-solubilizing bacteria (IPB) and organic P-mineralizing bacteria (OPB) were counted using the traditional colony-forming unit (CFU) method [25]. Five grams of sediment were mixed with 45 mL of deionized sterilized water in the flask with several glass beads and shook vigorously for 20 min. A 10-fold serial dilution of the suspension was prepared in sterilized water, and 200 μL of diluted sample was inoculated into organic P medium with egg yolk being the sole P source and inorganic P medium in which calcium phosphate was the sole P source. OPB and IPB colonies were counted after culturing at 28 °C for two and four days, respectively.

2.5. Statistical Analysis

Pearson's correlation coefficient analyses were carried out using SPSS statistical software version 20.0. The significance of differences among variables was determined via a *t*-test, $P < 0.05$ showed a significant difference or correlation. Maps were performed with ArcMap 10.2 version and figures were plotted in Origin 9.1 version.

3. Results

3.1. Abundance and Distribution of Phytoplankton

A total of 30 phytoplankton genera in 4 phyla were identified in the studied area of TWS, among which there were 19 genera of diatoms, 9 of dinoflagellates, 1 of cyanobacteria, and 1 of chrysophyceae. A significant difference in phytoplankton composition was observed between the northern and southern regions. *Prorocentrum* and *Chaetoceros* were the dominant groups with the mean abundance of 2.4×10^4 cells/L in the northern region, while the southern region was dominated by *Trichodesmium* and *Rhizosolenia* with the mean abundance of 3.7×10^4 cells/L. The abundances of *Prorocentrum* and *Chaetoceros* in the north were significantly higher than those in the south, while the relationship was reversed in terms of the abundance of *Rhizosolenia* ($P < 0.05$). *Trichodesmium* could only be observed in the southern region (Figure 2a).

In addition to directional spatial distribution, a distinct phytoplankton community was also observed between the coast and center in the strait. In detail, the abundance of *Prorocentrum* in the coast was significantly higher than that of the center in the north, while *Trichodesmium* was much more abundant in the center of the southern region ($P < 0.05$, Figure 2b).

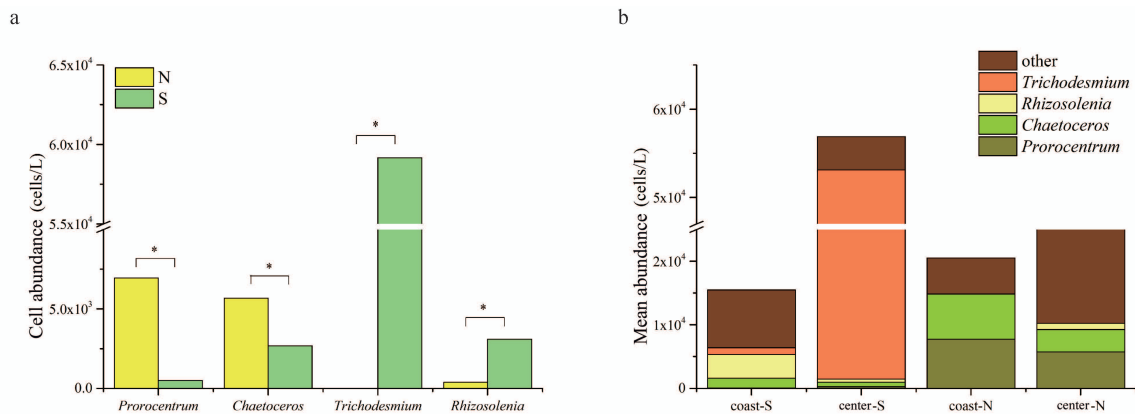


Figure 2. Differences in the abundance of dominant phytoplankton taxa between the Northern and Southern region (a), and between the coast and center (b) in Taiwan Strait.

3.2. Nutrient Distribution and Its Relationship with Phytoplankton Community

Significant differences were observed in the northern and southern surface waters in both concentrations of NO_2^- and NH_4^+ ($P < 0.01$, Table 1aa), which were abundant in the north and south, respectively. There was no significant difference in SRP concentrations between the south and north. Consequently, NH_4^+ /SRP ratio was significantly higher in the southern region ($P < 0.05$, Table 1aa).

Comparing with the center, concentrations of NO_3^- and DIN in the surface water of the coast in the northern region were significantly higher while TN concentration was significantly lower ($P < 0.05$, Table 1ab). In the southern region, concentrations of SRP, TP, NO_3^- , DIN, and TN in the bottom water of the center were significantly higher than those in the coast ($P < 0.05$), while the ratios of TN/TP, DIN/SRP, and NH_4^+ /SRP were significantly lower there ($P < 0.05$, Table 1ab). Chl *a* concentration, the abundances of *Prorocentrum* and dinoflagellates were negatively correlated with NH_4^+ in surface water ($P < 0.05$, Figure 3b).

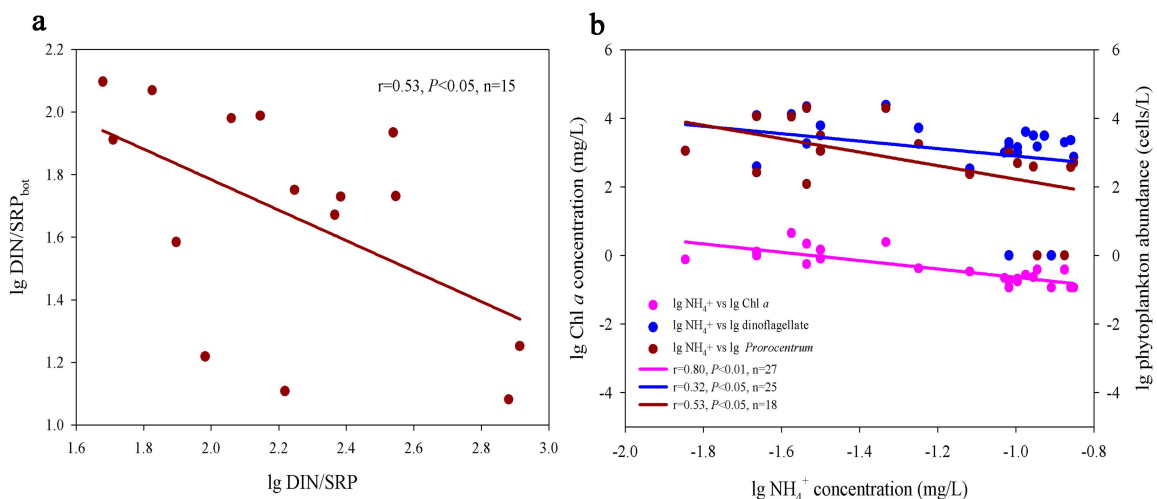


Figure 3. Correlations between the dissolved inorganic N and ammonium to soluble reactive P (DIN/SRP) ratio in surface and bottom water of southern region (a), correlations between Chl *a*, abundance of dinoflagellate and *Prorocentrum*, and NH_4^+ concentrations in surface water of Taiwan Strait (b).

Table 1a. Differences in nutrient concentrations among the sampling stations in the southern (S) and northern (N) regions.

Types	Regions	SRP	TP	NO ₃ ⁻	NO ₂ ⁻	NH ₄ ⁺	DIN	TN	TN/TP	DIN/SRP	NH ₄ ⁺ /SRP
Surface	S	0.005 ± 0.003	0.021 ± 0.014	0.474 ± 0.049	0.000 ± 0.001**	0.110 ± 0.018 **	0.584 ± 0.050	3.250 ± 0.340	187.033 ± 63.279	245.934 ± 233.053	45.579 ± 44.957 *
	N	0.007 ± 0.006	0.027 ± 0.016	0.481 ± 0.120	0.056 ± 0.022	0.031 ± 0.012	0.568 ± 0.129	3.415 ± 0.134	158.590 ± 66.362	144.464 ± 122.623	8.903 ± 7.531
Bottom	S	0.023 ± 0.027	0.035 ± 0.024	0.563 ± 0.179	0.003 ± 0.005	0.082 ± 0.014	0.648 ± 0.176	3.093 ± 0.377	124.750 ± 57.570	60.738 ± 36.709	9.143 ± 6.290
	N	-	-	-	-	-	-	-	-	-	-
Interstitial	S	-	-	-	-	-	-	-	-	-	-
	N	0.075 ± 0.014	-	0.976 ± 0.448	0.009 ± 0.005	1.538 ± 0.500	2.523 ± 0.456	-	-	34.610 ± 7.032	20.543 ± 5.081

* for $P < 0.05$; ** for $P < 0.01$.

Table 1b. Differences in nutrient concentration among the sampling stations at the coast and center.

Regions	Types	Shore	SRP	TP	NO ₃ ⁻	NO ₂ ⁻	NH ₄ ⁺	DIN	TN	TN/TP	DIN/SRP	NH ₄ ⁺ /SRP
S	Surface	coast	0.006 ± 0.004	0.026 ± 0.020	0.453 ± 0.067	0.0003 ± 0.001	0.108 ± 0.013	0.561 ± 0.055	3.135 ± 0.325	164.55 ± 55.580	162.98 ± 106.410	29.804 ± 17.694
		center	0.004 ± 0.003	0.018 ± 0.006	0.488 ± 0.022	0.0005 ± 0.001	0.111 ± 0.020	0.599 ± 0.039	3.326 ± 0.327	202.02 ± 63.661	301.24 ± 274.459	56.096 ± 53.696
	Bottom	coast	0.007 ± 0.002 *	0.017 ± 0.003 *	0.444 ± 0.040 *	0.000 ± 0.001	0.084 ± 0.011	0.528 ± 0.049 *	2.836 ± 0.293 *	167.418 ± 35.900 *	83.009 ± 24.161 *	13.147 ± 3.854 *
		center	0.034 ± 0.030	0.046 ± 0.025	0.643 ± 0.190	0.005 ± 0.006	0.081 ± 0.015	0.728 ± 0.184	3.264 ± 0.326	96.304 ± 51.398	45.891 ± 36.133	6.473 ± 6.183
	Interstitial	coast	-	-	-	-	-	-	-	-	-	-
		center	-	-	-	-	-	-	-	-	-	-
N	Surface	coast	0.009 ± 0.007	0.026 ± 0.007	0.548 ± 0.086 *	0.064 ± 0.010	0.030 ± 0.013	0.642 ± 0.091 *	3.343 ± 0.083 *	136.554 ± 30.631	102.27 ± 52.869	5.639 ± 4.175
		center	0.004 ± 0.003	0.029 ± 0.023	0.381 ± 0.089	0.045 ± 0.030	0.032 ± 0.009	0.458 ± 0.094	3.524 ± 0.123	191.64 ± 88.213	207.76 ± 163.466	13.800 ± 8.700
	Bottom	coast	-	-	-	-	-	-	-	-	-	-
		center	-	-	-	-	-	-	-	-	-	-
	Interstitial	coast	0.070 ± 0.009	-	1.028 ± 0.474	0.008 ± 0.004	1.418 ± 0.462	2.454 ± 0.470	-	-	35.729 ± 7.199	20.324 ± 5.540
		center	0.099 ± 0.000	-	0.715 ± 0.000	0.014 ± 0.000	2.138 ± 0.000	2.868 ± 0.000	-	-	29.013 ± 0.000	21.646 ± 0.000

* for $P < 0.05$.

3.3. Phytoplankton Extracellular Alkaline Phosphatase

ELF active cells indicating excretion of extracellular APase in phytoplankton were detected in each studied transect, belong to genera of *Prorocentrum*, *Scrippsiella*, and *Neoceratium* belonging to dinoflagellates, *Thalassionema*, *Skeletonema*, *Pleurosigma* and *Cyclotella* belonging to diatoms, and *Trichodesmium* belonging to cyanobacteria (Figure 4). The percentage of ELF-labeling cells in different transects fluctuated from 1.47% to 66.67% with a mean of 38.04% (Table 2).

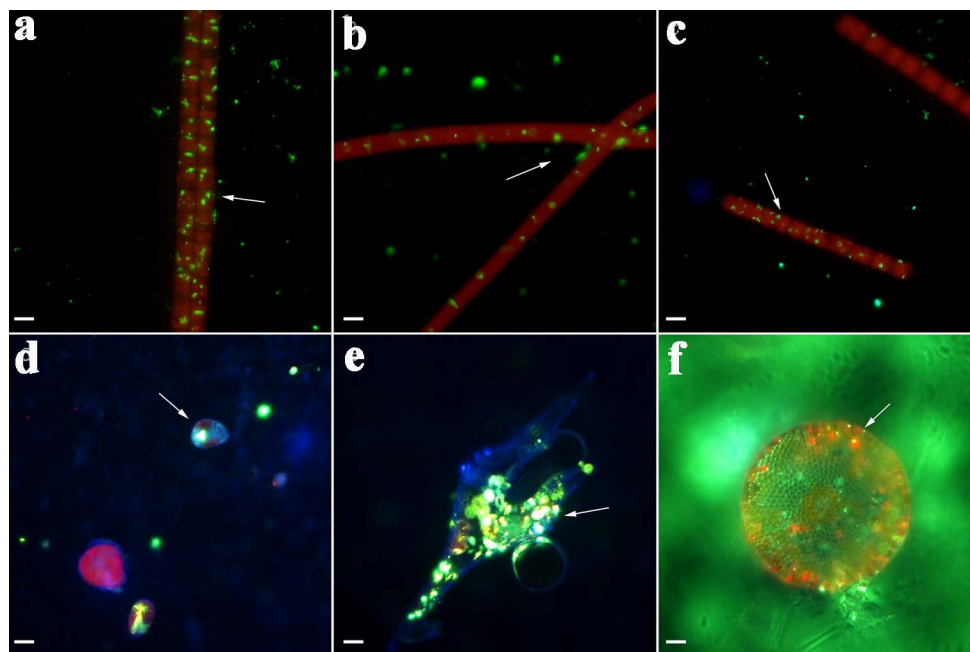


Figure 4. Microscopic observations of in situ response of phytoplankton. Fresh phytoplankton samples were treated with enzyme-labelled fluorescence (ELF) reagent for extracellular phosphatase detection. Green fluorescence ELF-labelling associated with cells was observed. (a–c) *Trichodesmium* sp. from transects A, B, and C. (d–f) *Prorocentrum* sp., *Ceratium* sp. and *Coscinodiscus* sp. from transaction D. Scale bars indicate 10 μm.

Table 2. Elf-labeling cells of the sampling stations in the southern region.

Station	A1	A2	A3	A6	A7	B1	B3	B5	B6	C1	C4
ELF (%)	65.49	40.31	63.38	25.59	24.81	28.72	26.79	11.53	1.48	63.64	66.67

3.4. Nutrient Status in Surface and Bottom Water

In the southern region, the ratios of DIN/SRP in the surface and bottom water were negatively correlated ($P < 0.05$, Figure 3a). Though the percentage of ELF-labeling cells in *Trichodesmium* was negatively correlated with TP and SRP concentrations ($P < 0.05$, Figure 5c), it showed positive relationships with ratios of TN/TP, DIN/SRP, and NH_4^+ /SRP in the bottom water ($P < 0.05$, Figure 5d). Furthermore, the abundances of phytoplankton and *Trichodesmium* were negatively correlated with the ratios of DIN/SRP and NH_4^+ /SRP in the bottom water ($P < 0.05$, Figure 5a,b).

CaCO₃~P was the main form of P in the sediment in the northern region, followed by Fe(OOH)~P. The contents of different forms of P and Q_{max} of P in transect D were significantly lower than those in transects E and F ($P < 0.05$, Figure 6a,b). In terms of PSB, the abundance of IPB in the sediment was significantly higher than that of OPB ($P < 0.05$, Figure 6c,d), and the former was positively correlated with NO₃⁻ in the interstitial water ($P < 0.05$, Figure 7). The abundances of OPB and IPB in transect D were higher than those in transects E and F.

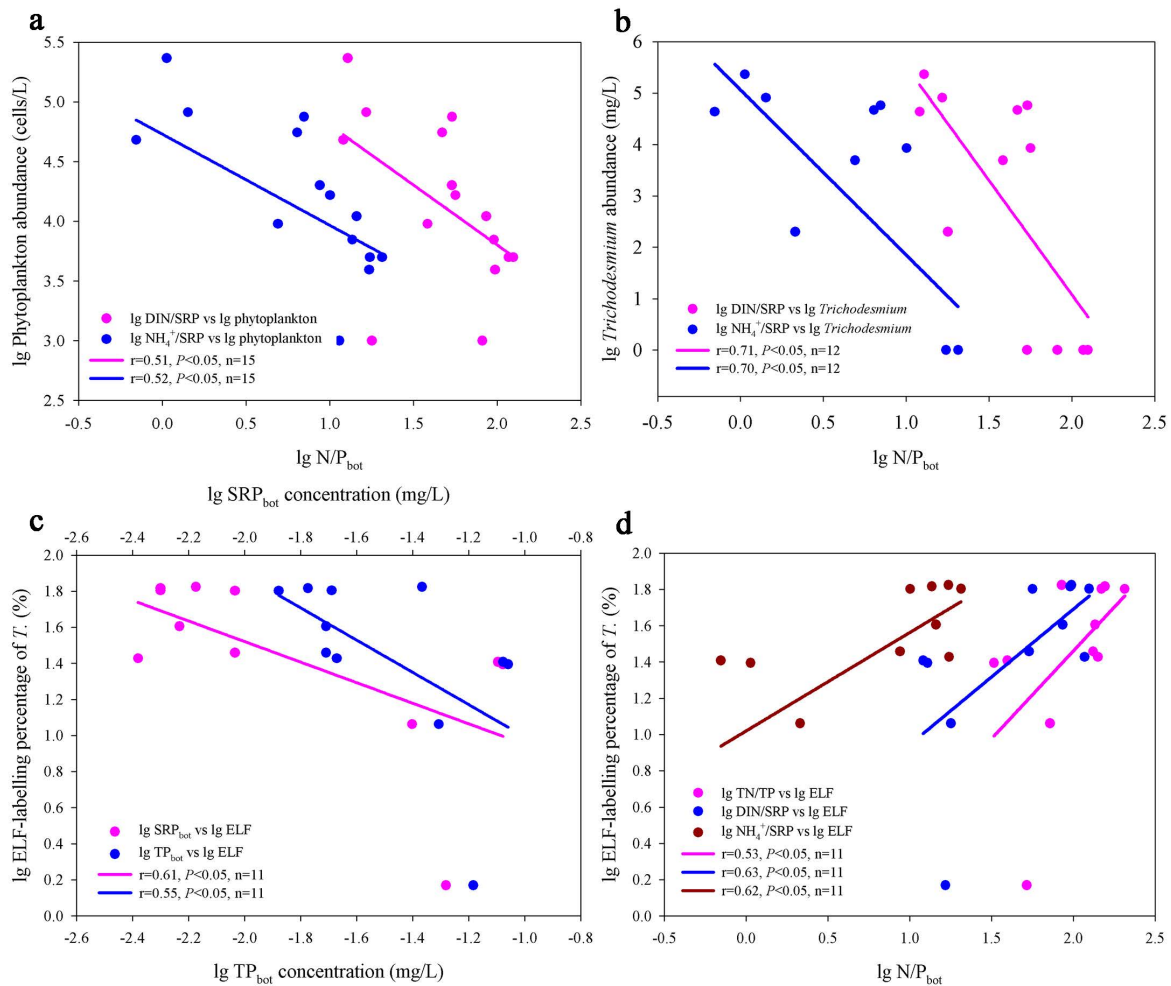


Figure 5. Correlations between phytoplankton abundance in surface water and inorganic N/P ratio in bottom water (a), the abundance of *Trichodesmium* in surface water and inorganic N/P ratio in bottom water (b), percentage of ELF-labelling cells in *Trichodesmium* and total phosphorus (TP), SRP concentrations in bottom water (c) and percentage of ELF-labelling cells in *Trichodesmium* and N/P ratio in bottom water (d).

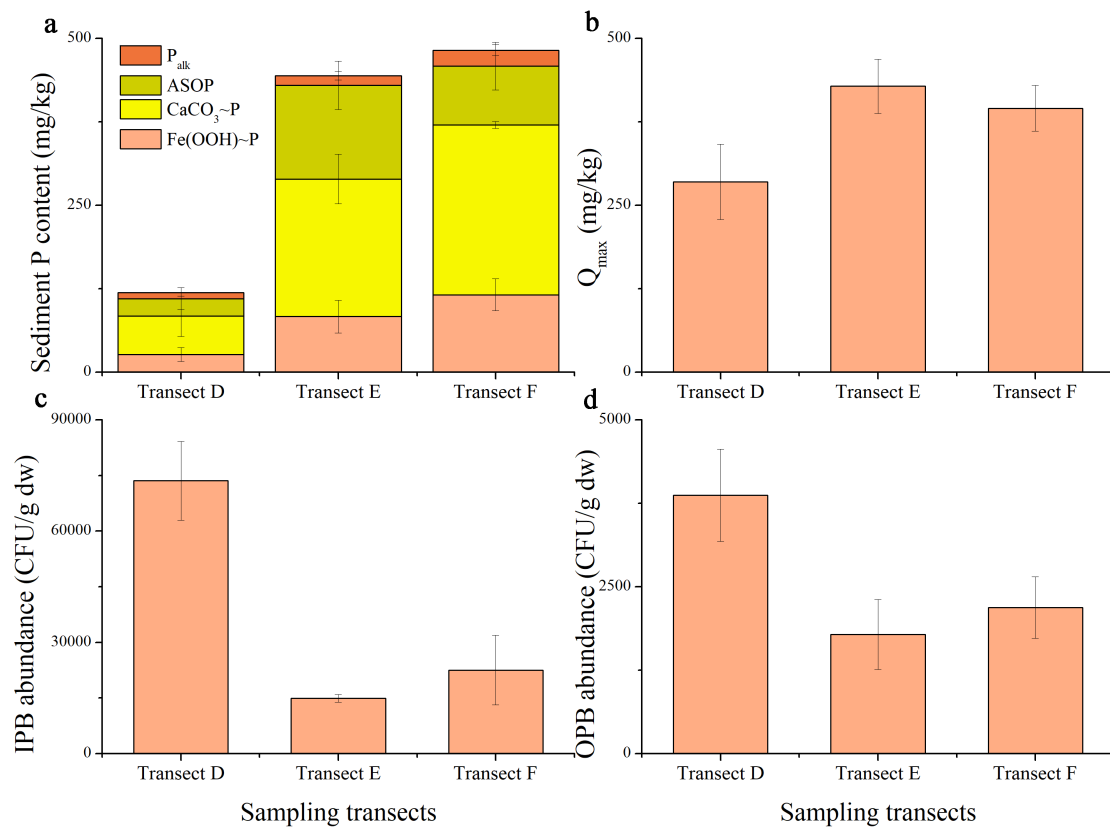


Figure 6. Different forms of P content (a), Q_{max} (b), inorganic P-solubilizing bacteria (IPB) (c), and organic P-mineralizing bacteria (OPB) abundance (d) in the sediment in the northern region of Taiwan Strait.

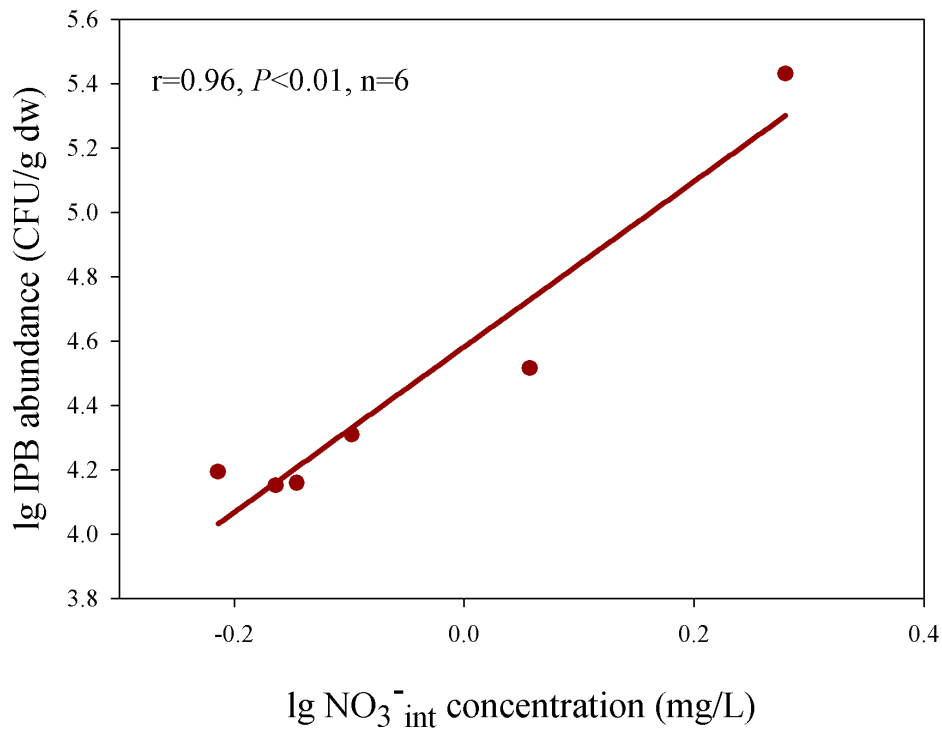


Figure 7. Correlation between sediment IPB abundance and NO_3^- concentration in interstitial water.

4. Discussion

It was widely accepted that the distribution of macronutrients, such as N and P shaped the phytoplankton assemblage and its succession, but the underlying mechanism in nutrient transfer and the coupling between the physiological responses of phytoplankton and nutrient supply remain largely unknown. Despite the important location of TWS, the structure of the phytoplankton community and its relationship with the nutrient regime were rarely investigated, especially in spring. In the current study, an imbalanced nutrient profile and corresponding spatial heterogeneity of the phytoplankton community were observed. An abundance of cyanobacterial *Trichodesmium* reaching almost red tide threshold was reported in the southern region of TWS. We proposed that the distribution was owing to its vertical migration and benthic nutrient regime since the abundance and extracellular APase of *Trichodesmium* were both regulated by benthic P concentration and the ratio of N/P. The pelagic-benthic coupling was emphasized.

4.1. Spatial Heterogeneity of Phytoplankton Community in the Taiwan Strait

Our results reported the distribution of the phytoplankton community in the TWS in spring 2018. A horizontal and transect patchy distribution of phytoplankton was observed in the northern and southern regions, which was previously described in the coastal upwelling zone of the western TWS in summer [2]. Particular attention should be given to two genera of *Prorocentrum* and *Trichodesmium*, dominating phytoplankton assemblage of the northern and southern regions, respectively. Despite the abundance of dinoflagellate was not high, the species number was diverse. Notably, the abundance of *Prorocentrum* on the coast was significantly higher than that in the center region ($P < 0.05$, Figure 2b). Consistent with our observation, it was recently reported that *Prorocentrum* only appeared at the coast stations in the northern TWS [26]. *Trichodesmium* is a typical red tide causing and N_2 -fixing cyanobacteria, which was reported in the center of TWS in the last decades [2,15,27]. In this study, the highest abundance of *Trichodesmium* reached 2.3×10^5 cells/L in the southern region of the strait. Though it was lowered than the speculative red tide threshold (1.0×10^6 cells/L) described by Adachi [28], and saxitoxin congeners and microcystins may not represent potential harm to human health by primary contact, the toxins were present at low concentrations in *Trichodesmium* blooms toxins [29]. Special attention should be paid to it to avoid the potential risk of red tide.

4.2. Spatial Heterogeneity of Phytoplankton Community in Response to the Imbalanced Distribution of N and P

A possible explanation for the spatial heterogeneity of the phytoplankton community might attribute to the imbalanced distribution of N and P. For example, abundances of *Prorocentrum* and *Chaetoceros* were always accompanied by significantly higher NO_2^- but lower NH_4^+ concentrations. In general, Chl *a* concentration, abundances of dinoflagellates and *Prorocentrum* were negatively correlated with NH_4^+ concentration ($P < 0.05$, Figure 3b). Preferential absorbance of NH_4^+ by the algae might lead to the negative relationship between the algal abundance and ambient NH_4^+ concentration. The concentration of NH_4^+ was higher than that of NO_3^- and NO_2^- in the cells of *Prorocentrum* in the culture [30]. Furthermore, NO_2^- concentration in the northern region was significantly higher than that in the south ($P < 0.05$, Table 1aa). Notably, *Prorocentrum* could absorb and utilize NH_4^+ and release NO_2^- in the culture medium [31], which further interpreted the negative correlation between algal abundance versus NH_4^+ and significant difference of NO_2^- between the south and the north. Similar to *Prorocentrum*, *Chaetoceros* preferentially absorbs NH_4^+ , but its utilization is saturated [32]. Consequently, the patch of the phytoplankton community was formed in response to the distribution of various DIN.

Our results also pointed at variations of P in regulating the structure of the phytoplankton community. For example, we found a significantly higher ratio of NH_4^+ /SRP concomitantly with the higher abundances of *Rhizosolenia* and *Trichodesmium* in the southern region (Table 1aa, Figure 2a), indicating they might overcome P deficiency since a high ratio of NH_4^+ /SRP indicates the P deficiency.

Exuding extracellular APase that release DIP from dissolved organic phosphorus (DOP) compounds is an important strategy for phytoplankton to overcome P limitation. In this study, the proportion of ELF active cells in *Trichodesmium erythraea* could be up to 65% in the southern region (Table 2). Consistent with this observation, the percentages of ELF active cells in *Trichodesmium* of North Pacific were 100% [33], and 81% of alkaline phosphatase activities (APA) was contributed by *Trichodesmium* in Bermuda Atlantic [34]. *Trichodesmium* could meet its P demand by relying on DOP since it was weak in competing DIP with co-occurring phytoplankton [35]. Similar to *Trichodesmium*, *Rhizosolenia* could secrete APase to overcome P limitation [15]. The predominant species may shift from smaller or chain-forming diatoms such as *Skeletonema costatum* and *Thalassiosira subtilis* to large diatoms like *Rhizosolenia* with the nutrient declining [36], indicating *Rhizoctonia* could adapt to the P-deficient ambient.

Overcoming P limitation by excreting extracellular APase also could be seen in *Ceratium*, *Prorocentrum*, and *Coscinodiscus* in the transect D with a significantly higher ratio of NH_4^+/SRP (Figure 4). APA and surplus cellular P in *Ceratium* fluctuated with the ambient P supply in the eutrophic Eau Galle Reservoir [37]. In addition to secreting APase to overcome P deficiency, *Prorocentrum* can complement DIP by DOP such as ATP by stopping DNA duplication or check-point protein phosphorylation [38]. *Coscinodiscus* also presented a higher specific APA in P limited cultures [39]. Therefore, the relative abundance and deficiency of available P and the physiological response strategy shaped the patchy distribution pattern of the phytoplankton community in the TWS.

4.3. The Relationship between Bottom Nutrient Status and Spatial Heterogeneity of Phytoplankton Community

An opposite DIN/SRP ratio was observed in the TWS with high value on the surface while low in the bottom ($P < 0.05$, Figure 3a). A similar imbalanced reversal vertical distribution of N and P was also found in the Adriatic Sea [40]. This reversal distribution could be interpreted in biogeochemical nutrient cycling and the response and feedback to nutrients by phytoplankton.

It was expected a lower DIN/SRP ratio which indicated N deficiency in the bottom as N was preferentially consumed [41]. Various ways of P release in the sediment might aggravate the N deficiency in the bottom. For example, the release of P from anoxic coastal sediment led to a decrease in DIN/SRP ratio in the overlying water [42]. $\text{Fe}(\text{OOH})\sim\text{P}$ played a vital role in sequestering sedimentary P [43]. In the current study, the main form of P in the sediments of TWS was $\text{CaCO}_3\sim\text{P}$, not $\text{Fe}(\text{OOH})\sim\text{P}$, suggesting a weak sequestration of P from the water. Furthermore, $\text{CaCO}_3\sim\text{P}$ could be also a potential P source [43]. PSB could release a great deal of bioavailable P by solubilizing Ca_3PO_4 [44]. An abundance of IPB, which can dissolve $\text{CaCO}_3\sim\text{P}$, was detected in the transect D (Figure 6c). Interestingly, the abundance of IPB was significantly positively correlated with the concentration of NO_3^- in the interstitial water ($P < 0.05$, Figure 7). The application of NO_3^- could promote mycorrhizal colonization and hyphal length abundance of PSB [45]. In addition, a significantly lower P content and Q_{\max} in the transect D contributed to its lower ratio of NH_4^+/SRP in the interstitial water. Shortly, weak retention capacity and strong release potential resulted in the lower DIN/SRP ratio in the interstitial water.

The distinct uptake and feedback to ambient P and N by various phytoplankton could change the composition of the nutrient pool greatly. Phytoplankton could luxuriously uptake P, resulting in a rapid drawdown in DIP relative to DIN in the euphotic zone [46]. *Trichodesmium* contributed a considerable source of N to the euphotic zones of the tropical and subtropical regimes by N_2 -fixation [47]. A high NH_4^+ concentration in the surface of the southern TWS might be due to the N_2 -fixation by *Trichodesmium* and *Rhizosolenia*, which are actually diatom-diazotroph associations. Beyond the expectation, *Rhizosolenia fragilissima* was flourished by P deficient conditions [48]. N_2 -fixation rates of *Trichodesmium* were found negatively correlated with DIP concentrations but positively correlated with APase activity [49]. In summary, the reversal of the N/P ratio from the bottom to the surface was to some extent owing to the rapid absorb of P and substantial contribution to N by phytoplankton.

An interesting significant relationship between pelagic phytoplankton and benthic nutrient was observed in our study. Specifically, the abundance of *Trichodesmium* and the ratio of inorganic N and P (including NH_4^+/SRP and DIN/SRP) in the bottom water were significantly negatively correlated

($P < 0.05$, Figure 5b). Furthermore, the percentage of *Trichodesmium* with ELF-labeling cells was not only negatively correlated with the benthic concentrations of SRP and TP but also positively correlated with different inorganic forms of N/P ratio ($P < 0.05$, Figure 5c,d). These relationships indicated the benthic origin of surface *Trichodesmium*. *Trichodesmium* in the TWS was reported in the summer of 2015, which was assumed to be the advection intrusion from Kuroshio Current [27]. The bottom water in TWS could be originated from the intrusive Kuroshio subsurface water [50]. The reasons as to the pelagic and benthic coupling could be either attributed to the matter transformation in the upwelling. For example, *Trichodesmium* could be brought to the surface by upwelling in the western TWS [51]. Surface *Trichodesmium* populations were supplied by the Loop Current from coast-bottom in the Gulf of Mexico [52]. We excluded this possibility in our scenario as the stations dominated with *Trichodesmium* were located in the center region of the strait were not at the upwelling region. It is likely that a low ratio of N/P in the bottom triggered *Trichodesmium* bloom and vertically migrated to the surface, which could help to explain the regulation of extracellular APase by the benthic P. Actually, *Trichodesmium* bloom could be triggered by a supply of high concentrations of N, P and low N/P ratio [53]. The maximum ascent and sinking rate of *Trichodesmium* could be up to 6.1 m/hr [54]. N scarcity was usually associated with increased abundance of *Trichodesmium* even in the depth of 450 m in the sea [55]. *Trichodesmium* might migrate to the P replete bottom and return to the surface for photosynthesis and N_2 -fixation [56]. Molecular N and P ratio were differences ($P < 0.001$) significantly in the western Gulf of Mexico between sinking and ascending *Trichodesmium* (87.0 and 43.5, respectively) and provided the best direct evidence to date of vertical migration for P acquisition [57]. Besides, mesoscale eddies could affect nitrogen fixation by affecting nutrient availability and eddy transport, which are associated with N_2 -fixing cyanobacteria *Trichodesmium* [58]. *Trichodesmium* also can be influenced by the occurrence of internal waves [59]. Shortly, the rapid prosper of *Trichodesmium* in recent years may have great ecological implications to the TWS. The reasons for its surface bloom remain unknown and merit further and dedicated research.

5. Conclusions

A patching phytoplankton community distribution was observed in the TWS owing to the imbalanced nutrient regimes and nutrient scavenging strategies. Dominant phytoplankton, e.g., *Trichodesmium*, whose abundance reached almost red tide threshold in the southern region of TWS, might overcome P deficiency by exuding extracellular APase. The growth and biochemical response of *Trichodesmium* were regulated by the benthic nutrient supply, indicating that the benthic nutrient regime could shape the structure of the pelagic phytoplankton community.

Supplementary Materials: The following are available online at <http://www.mdpi.com/2077-1312/8/10/807/s1>, Table S1: The water depth among the sampling sites.

Author Contributions: All the authors contributed to the study conception and design. Conceptualization, L.S., Y.Z., and X.C. (Xiuyun Cao); formal analysis, X.L., X.C. (Xiaojie Chai), L.Z., Q.D., X.C. (Xiaoyan Chen), Q.Z. and L.W.; funding acquisition, C.S., L.S., Y.Z., and X.C. (Xiuyun Cao); investigation, X.L., X.C. (Xiaojie Chai), L.Z., Q.D., X.C. (Xiaoyan Chen), Q.Z., and L.W.; methodology, X.L., X.C. (Xiaojie Chai) and X.C. (Xiaoyan Chen); supervision, L.S., Y.Z., and X.C. (Xiuyun Cao); writing—original draft, X.L., X.C. (Xiaojie Chai) and X.C. (Xiuyun Cao); writing—review and editing, C.S., L.S., Y.Z., and X.C. (Xiuyun Cao). All authors have read and agreed to the published version of the manuscript.

Funding: This research was funded by the National Key Research and Development Program of China, grant number 2016YFE0202100, Natural Science Foundation of China, grant number 41877381, and the State Key Laboratory of Freshwater Ecology and Biotechnology, grant number 2019FBZ01.

Conflicts of Interest: The authors declare no conflict of interest.

References

1. Schrope, M. Oceanography: Red Tide rising. *Nature* **2008**, *452*, 24–26. [CrossRef]
2. Wang, Y.; Mang, J.H.; Ye, Y.Y.; Lin, G.M.; Yang, Q.L.; Lin, M. Phytoplankton community and environmental correlates in a coastal upwelling zone along western Taiwan Strait. *J. Mar. Syst.* **2016**, *154*, 252–263. [CrossRef]

3. Moore, C.M.; Mills, M.M.; Arrigo, K.R.; Berman-Frank, I.; Bopp, L.; Boyd, P.W.; Galbraith, E.D.; Geider, R.J.; Guieu, C.; Jaccard, S.L.; et al. Processes and patterns of oceanic nutrient limitation. *Nat. Geosci.* **2013**, *6*, 701–710. [[CrossRef](#)]
4. Hamilton, D.P.; Douglas, G.B.; Adeney, J.A.; Radke, L.C. Seasonal changes in major ions, nutrients and chlorophyll a at two sites in the Swan River estuary, Western Australia. *Mar. Freshw. Res.* **2006**, *57*, 803–815. [[CrossRef](#)]
5. Weston, K.; Fernand, L.; Mills, D.K.; Delahunty, R.; Brown, J. Primary production in the deep chlorophyll maximum of the centre North Sea. *J. Plankton. Res.* **2005**, *27*, 909–922. [[CrossRef](#)]
6. Liu, D.Y.; Shen, X.H.; Di, B.P.; Shi, Y.J.; Keesing, J.K.; Wang, Y.J.; Wang, Y.Q. Palaeoecological analysis of phytoplankton regime shifts in response to coastal eutrophication. *Mar. Ecol. Prog. Ser.* **2013**, *475*, 1–14. [[CrossRef](#)]
7. Wu, G.F.; Zhou, X.P. Characterization of phosphorus-releasing bacteria in a small eutrophic shallow, Eastern Lake. *Water Res.* **2005**, *39*, 4623–4632. [[CrossRef](#)]
8. Schindler, D.W.; Hecky, R.E.; Findlay, D.L.; Stainton, M.P.; Parker, B.R.; Paterson, M.J.; Beaty, K.G.; Lyng, M.; Kasian, S.E.M. Eutrophication of lakes cannot be controlled by reducing nitrogen input: Results of a 37-year whole-ecosystem experiment. *Proc. Natl. Acad. Sci. USA* **2008**, *105*, 11254–11258. [[CrossRef](#)]
9. Van Mooy, B.A.S.; Rocap, G.; Fredricks, H.F.; Evans, C.T.; Devol, A.H. Sulfolipids dramatically decrease phosphorus demand by picocyanobacteria in oligotrophic marine environments. *Proc. Natl. Acad. Sci. USA* **2006**, *103*, 8607–8612. [[CrossRef](#)] [[PubMed](#)]
10. Martin, P.; Dyhrman, S.T.; Lomas, M.W.; Poulton, N.J.; Van Mooy, B.A.S. Accumulation and enhanced cycling of polyphosphate by Sargasso Sea plankton in response to low phosphorus. *Proc. Natl. Acad. Sci. USA* **2014**, *111*, 8089–8094. [[CrossRef](#)]
11. Zhang, S.F.; Yuan, C.J.; Chen, Y.; Lin, L.; Wang, D.Z. Transcriptomic response to changing ambient phosphorus in the marine dinoflagellate *Prorocentrum donghaiense*. *Sci. Total Environ.* **2019**, *692*, 1037–1047. [[CrossRef](#)] [[PubMed](#)]
12. Ou, L.J.; Huang, B.Q.; Lin, L.; Hong, H.; Zhang, F.; Chen, Z. Phosphorus stress of phytoplankton in the Taiwan Strait determined by bulk and single-cell alkaline phosphatase activity assays. *Mar. Ecol. Prog. Ser.* **2006**, *327*, 95–106. [[CrossRef](#)]
13. Marine Environment Status Bulletin in China 2016. China Oceanic Information Network. Available online: <http://www.nmdis.org.cn/hygb/zgchyhjzlgb/2016nzgchyhjzkgb/> (accessed on 13 April 2017).
14. Hu, J.; Liu, X.; Zhang, F.; Huang, B.Q.; Hong, H.S. Study on nutrient limitation of phytoplankton in southern Taiwan Strait during the summer. *J. Oceanogr. Taiwan Strait* **2008**, *27*, 452–458. [[CrossRef](#)]
15. Dyhrman, S.T.; Palenik, B. Phosphate stress in cultures and field populations of the dinoflagellate *Prorocentrum minimum* detected by a single-cell alkaline phosphatase assay. *Appl. Environ. Microb.* **1999**, *65*, 3205–3212. [[CrossRef](#)] [[PubMed](#)]
16. Guo, H. *Illustrations of Planktons Responsible for the Blooms in Chinese Coastal Water*, 1st ed.; Science Press: Beijing, China, 2004.
17. González-Gil, S.; Keafer, B.A.; Jovine, R.V.M.; Aguilera, A.; Lu, S.H.; Anderson, D.M. Detection and quantification of alkaline phosphatase in single cells of phosphorus-starved marine phytoplankton. *Mar. Ecol. Prog. Ser.* **1998**, *164*, 21–35. [[CrossRef](#)]
18. Štrojsová, A.; Vrba, J.; Nedoma, J.; Komárková, J.; Znachor, P. Seasonal study on expression of extracellular phosphatase in the phytoplankton of a eutrophic reservoir. *Eur. J. Phycol.* **2003**, *38*, 295–306. [[CrossRef](#)]
19. Beattie, D.M.; Golterman, H.L.; Vijverberg, J. Introduction to limnology of Friesian lakes. *Hydrobiology* **1978**, *58*, 49–64. [[CrossRef](#)]
20. Greenberd, A.E.; Clesceri, L.S.; Eaton, A.D. *Standard Methods for the Examination of Water and Wastewater*, 22nd ed.; American Public Health Association: Washington, DC, USA, 2012.
21. Murphy, J.; Riley, J.P. A modified single solution method for determination of phosphate in natural waters. *Anal. Chim. Acta.* **1962**, *26*, 31–36. [[CrossRef](#)]
22. Golterman, H.L. Fractionation of sediment phosphate with chelating compounds: A simplification, and comparison with other methods. *Hydrobiologia* **1996**, *335*, 87–95. [[CrossRef](#)]
23. Istvanovics, V. Fractional composition, adsorption and release of sediment phosphorus in the Kis-Balaton reservoir. *Water Res.* **1994**, *28*, 717–726. [[CrossRef](#)]

24. Sakadevan, K.; Bavor, H.J. Phosphate adsorption characteristics of soils, slags and zeolite to be used as substrates in constructed wetland systems. *Water Res.* **1998**, *32*, 393–399. [[CrossRef](#)]
25. Nautiyal, C.S. An efficient microbiological growth medium for screening phosphate solubilizing microorganisms. *Fems. Microbiol. Lett.* **1999**, *170*, 265–270. [[CrossRef](#)] [[PubMed](#)]
26. Cen, J.Y.; Ou, L.J.; Li, S.; Zhang, H.; Wang, J.Y.; Lu, S.H. The species composition of dinoflagellate and its role of indication to Kuroshio and adjacent waters in spring 2014. *Sci. Rep.* **2017**, *48*, 1022–1029. [[CrossRef](#)]
27. Wen, Z.Z.; Lin, W.F.; Shen, R.; Hong, H.Z.; Kao, S.J.; Shi, D.L. Nitrogen fixation in two coastal upwelling regions of the Taiwan Strait. *Sci. Rep.* **2017**, *7*. [[CrossRef](#)]
28. Adachi, R. Red tide biology and red tide ecology. *Aquat. Archit.* **1973**, *9*, 31–36.
29. Proenca, L.A.O.; Tamanaha, M.S.; Fonseca, R.S. Screening the Toxicity and Toxin Content of Blooms of the Cyanobacterium *Trichodesmium Erythraeum* (Ehrenberg) In Northeast Brazil. *J. Venom. Anim Toxins* **2009**, *15*, 204–215. [[CrossRef](#)]
30. Lourenco, S.O.; Barbarino, E.; Marquez, U.M.L.; Aidar, E. Distribution of intracellular nitrogen in marine microalgae: Basis for the calculation of specific nitrogen-to-protein conversion factors. *J. Phycol.* **1998**, *34*, 798–811. [[CrossRef](#)]
31. Lomas, M.W.; Rumbley, C.J.; Glibert, P.M. Ammonium release by nitrogen sufficient diatoms in response to rapid increases in irradiance. *J. Plankton. Res.* **2000**, *22*, 2351–2366. [[CrossRef](#)]
32. Huang, L.D.; Wu, Y.D. Effects of dissolved inorganic nitrogen in water bodies on intracellular reactive nitrogen compounds of *Chaetoceros*. *J. Taiwan Strait* **1991**, *2*, 74–81.
33. Girault, M.; Arakawa, H.; Barani, A.; Ceccaldi, H.J.; Hashihama, F.; Kinouchi, S.; Gregori, G. Distribution of ultraphytoplankton in the western part of the North Pacific subtropical gyre during a strong La Nina condition: Relationship with the hydrological conditions. *Biogeosciences* **2013**, *10*, 5947–5965. [[CrossRef](#)]
34. Orcutt, K.M.; Gundersen, K.; Ammerman, J.W. Intense ectoenzyme activities associated with *Trichodesmium* colonies in the Sargasso Sea. *Mar. Ecol. Prog. Ser.* **2013**, *478*, 101–113. [[CrossRef](#)]
35. Sohm, J.A.; Capone, D.G. Phosphorus dynamics of the tropical and subtropical North Atlantic: *Trichodesmium* spp. versus bulk plankton. *Mar. Ecol. Prog. Ser.* **2006**, *317*, 21–28. [[CrossRef](#)]
36. Wang, Z.H.; Zhao, J.G.; Zhang, Y.J.; Cao, Y. Phytoplankton community structure and environmental parameters in aquaculture areas of Daya Bay, South China Sea. *J. Environ. Sci China* **2009**, *21*, 1268–1275. [[CrossRef](#)]
37. James, B.R.; Rabenhorst, M.C.; Frigon, G.A. Phosphorus sorption by peat and sand amended with Iron-Oxides or steel wool. *Water Environ. Res.* **1992**, *64*, 699–705. [[CrossRef](#)]
38. Li, M.Z.; Li, L.; Shi, X.G.; Lin, L.X.; Lin, S.J. Effects of phosphorus deficiency and adenosine 5'-triphosphate (ATP) on growth and cell cycle of the dinoflagellate *Prorocentrum donghaiense*. *Harmful Algae* **2015**, *47*, 35–41. [[CrossRef](#)]
39. Peters, F.; Arin, L.; Marrase, C.; Berdalet, E.; Sala, M.M. Effects of small-scale turbulence on the growth of two diatoms of different size in a phosphorus-limited medium. *J. Marine Syst.* **2006**, *61*, 134–148. [[CrossRef](#)]
40. Ivancic, I.; Godrijan, J.; Pfannkuchen, M.; Maric, D.; Gasparovic, B.; Djakovac, T.; Najdek, M. Survival mechanisms of phytoplankton in conditions of stratification-induced deprivation of orthophosphate: Northern Adriatic case study. *Limnol. Oceanogr.* **2012**, *57*, 1721–1731. [[CrossRef](#)]
41. Connelly, T.L.; Deibel, D.; Parrish, C.C. Biogeochemistry of coast-bottom suspended particulate matter of the Beaufort Sea shelf (Arctic Ocean): C, N, P, delta C-13 and fatty acids. *Cont. Shelf Res.* **2012**, *43*, 120–132. [[CrossRef](#)]
42. Ingall, E.; Jahnke, R. Evidence for enhanced phosphorus regeneration from marine-sediments overlain by oxygen depleted waters. *Geochim. Cosmochim. Ac.* **1994**, *58*, 2571–2575. [[CrossRef](#)]
43. Kraal, P.; Dijkstra, N.; Behrends, T.; Slomp, C.P. Phosphorus burial in sediments of the sulfidic deep Black Sea: Key roles for adsorption by calcium carbonate and apatite authigenesis. *Geochim. Cosmochim. Ac.* **2017**, *204*, 140–158. [[CrossRef](#)]
44. Zhu, F.L.; Qu, L.Y.; Hong, X.G.; Sun, X.Q. Isolation and Characterization of a Phosphate-Solubilizing Halophilic Bacterium *Kushneria* sp. YCWA18 from Daqiao Saltern on the Coast of Yellow Sea of China. *Evid Based Compl. Alt.* **2011**, *2011*, 1–6. [[CrossRef](#)]
45. Ding, X.D.; Zhang, L.; Zhang, S.R.; Feng, G. Phytate utilization of maize mediated by different nitrogen forms in a plant-arbuscular mycorrhizal fungus-phosphate-solubilizing bacterium system. *J. Plant. Interact.* **2014**, *9*, 514–520. [[CrossRef](#)]

46. Mackey, K.R.M.; Mioni, C.E.; Ryan, J.P.; Paytan, A. Phosphorus cycling in the red tide incubator region of Monterey Bay in response to upwelling. *Front. Microbiol.* **2012**, *3*, 33. [[CrossRef](#)] [[PubMed](#)]
47. Montoya, J.P.; Holl, C.M.; Zehr, J.P.; Hansen, A.; Villareal, T.A.; Capone, D.G. High rates of N-2 fixation by unicellular diazotrophs in the oligotrophic. *Nature* **2004**, *430*, 1027–1031. [[CrossRef](#)] [[PubMed](#)]
48. Carlsson, P.; Graneli, E.; Segatto, A.Z. Cycling of biologically available nitrogen in riverine humic substances between marine bacteria, a heterotrophic nanoflagellate and a photosynthetic dinoflagellate. *Aquat. Microb. Ecol.* **1999**, *18*, 23–36. [[CrossRef](#)]
49. Bonnet, S.; Berthelot, H.; Turk-Kubo, K.; Fawcett, S.; Rahav, E.; L'Helguen, S.; Berman-Frank, I. Dynamics of N₂ fixation and fate of diazotroph-derived nitrogen in a low-nutrient, low-chlorophyll ecosystem: Results from the VAHINE mesocosm experiment (New Caledonia). *Biogeosciences* **2016**, *13*, 2653–2673. [[CrossRef](#)]
50. Yang, D.Z.; Yin, B.S.; Liu, Z.L.; Bai, T.; Qi, J.F.; Chen, H.Y. Numerical study on the pattern and origins of Kuroshio branches in the bottom water of southern East China Sea in summer. *J. Geophys. Res. Oceans* **2012**, *117*, C02014. [[CrossRef](#)]
51. Yu, S.J.; Gong, F.; He, X.Q.; Bai, Y.; Zhu, Q.K.; Wang, D.F.; Chen, P. Satellite views of the massive algal bloom in the Persian Gulf and the Gulf of Oman during 2008–2009. In *Remote Sensing of the Ocean, Sea Ice, Coastal Waters, and Large Water Regions 2016*; Charles, R.B., Xavier, N., Caroline, N., Oscar, A., Eds.; SPIE: Bellingham, WA, USA, 2016; Volume 9999, pp. 99990Z-1-99990Z-10. [[CrossRef](#)]
52. Walsh, J.B. A theoretical analysis of sliding of rough surfaces. *J. Geophys. Res.-Sol. Earth* **2003**, *108*. [[CrossRef](#)]
53. Rahav, E.; Bar-Zeev, E. Sewage outburst triggers *Trichodesmium* bloom and enhance N₂ fixation rates. *Sci. Rep.* **2017**, *7*. [[CrossRef](#)]
54. Walsby, A.F. The properties and buoyancy-providing role of gas vacuoles in *Trichodesmium* Ehrenberg. *Br. Phycol. J.* **1978**, *13*, 103–116. [[CrossRef](#)]
55. Böttger-Schnack, R.; Schnack, D. Vertical distribution and population structure of *Macrosetella gracilis* (Copepoda, Harpacticoida) in the Red Sea in relation to the occurrence of *Oscillatoria* (*Trichodesmium*) spp. (Cyanobacteria). *Mar. Ecol. Prog. Ser.* **1989**, *52*, 17–31. [[CrossRef](#)]
56. Karl, D.M.; Letelier, R.; Hebel, D.V.; Bird, D.F.; Winn, C.D. *Trichodesmium* Blooms and new nitrogen in the North Pacific Gyre. In *Marine Pelagic Cyanobacteria: Trichodesmium and other Diazotrophs*, NATO ASI Series C: *Mathematical and Physical Sciences*; Carpenter, E.J., Capone, D.G., Reuter, J.G., Eds.; Springer: Dordrecht, The Netherlands, 1992; Volume 362, pp. 219–237.
57. Villareal, T.A.; Carpenter, E.J. Buoyancy regulation and the potential for vertical migration in the oceanic cyanobacterium *Trichodesmium*. *Microb. Ecol.* **2003**, *45*, 1–10. [[CrossRef](#)]
58. Liu, J.X.; Zhou, L.B.; Li, J.J.; Lin, Y.Y.; Ke, Z.X.; Zhao, C.Y.; Liu, H.J.; Jiang, X.; He, Y.H.; Tan, Y.H. Effect of mesoscale eddies on diazotroph community structure and nitrogen fixation rates in the South China Sea. *Reg. Stud. Mar. Sci.* **2020**, *35*. [[CrossRef](#)]
59. Shiozaki, T.; Chen, Y.L.L.; Lin, Y.H.; Taniuchi, Y.; Sheu, D.S.; Furuya, K.; Chen, H.Y. Seasonal variations of unicellular diazotroph groups A and B, and *Trichodesmium* in the northern South China Sea and neighboring upstream Kuroshio Current. *Cont. Shelf Res.* **2014**, *80*, 20–31. [[CrossRef](#)]

Publisher's Note: MDPI stays neutral with regard to jurisdictional claims in published maps and institutional affiliations.



© 2020 by the authors. Licensee MDPI, Basel, Switzerland. This article is an open access article distributed under the terms and conditions of the Creative Commons Attribution (CC BY) license (<http://creativecommons.org/licenses/by/4.0/>).